SECTION 3

PHYSICS OF RADIATION AND ION-PLASMA TECHNOLOGIES

INFLUENCE OF THE MAGNITUDE OF THE BIAS POTENTIAL AND THICKNESS OF THE LAYERS ON THE STRUCTURE, SUBSTRUCTURE, STRESS-DEFORMED STATE AND MECHANICAL CHARACTERISTICS OF VACUUM-ARC MULTI-LAYERED (TiMo)N/(TiSi)N COATINGS

O.V. Sobol'[1], H.O. Postelnyk[1], A.A. Meylekhov[1], V.V. Subbotina[1], V.A. Stolbovoy[2], A.V. Dolomanov[2], D.A. Kolesnikov[3], M.G. Kovaleva[3], Yu.V. Sukhorukova[3]

[1]National Technical University "Kharkiv Polytechnic Institute", Kharkiv, Ukraine

E-mail: sool@kpi.kharkov.ua;

[2] National Science Center "Kharkov Institute of Physics and Technology", Kharkiv, Ukraine

E-mail: stolbovoy@kipt.kharkov.ua;

[3]Belgorod State National Research University, Belgorod, Russian Federation

E-mail: kolesnikovdmitry71@gmail.com

Layers based on titanium nitride doped with molybdenum and silicon were used to create a multilayer composite. In this case, the mismatch between the lattice periods of (TiMo)N and (TiSi)N layers was about 1%. It was found that in the (TiMo)N/(TiSi)N multilayer composite, such a mismatch of the periods in the constituent layers does not change the single-phase state of the composite even at relatively large layer thicknesses (about 350 nm). The creation of a (TiMo)N/(TiSi)N composite with a nanometer layer thickness allows one to reduce the magnitude of macrostresses (a large value of which is characteristic of single-layer (TiMo)N coatings) and change the substructural characteristics in a wide range of values. It has been established that the use of multi-element (TiMo)N and (TiSi)N layers in a multilayer coating design allows one to achieve a high-hard state with high adhesive strength and good tribological characteristics. The highest properties (hardness – 34.8 GPa and adhesive strength – 166.09 N) were achieved in coatings obtained at U_b = -200 V and a layer thickness of 80 nm, which are characterized by compression macrostresses of 7.85 GPa and microstrains – 0.75%.

PACS: 81.07.Bc, 61.05.sp, 68.55.jm, 61.82.Rx

INTRODUCTION

Recently, nitrides, carbides and oxides of transition metals are actively used in industry because of their high physical and mechanical properties. The most studied and common among them is titanium nitride. It has high hardness, wear resistance, corrosion resistance. However, at temperatures above 500 °C, significant disadvantages of titanium nitride are low – strength and oxidation stability [1].

To increase these characteristics, the concept of multi-element alloying is being developed. Al, Mo, Zr, Si, and others are used as alloying elements [2, 3]. It was established that the addition of Al increases the heat resistance, and Si increases the ability of the coating to resist abrasive wear [4]. Moreover, the TiSiN coating is characterized by high hardness (> 40 GPa), resistance to oxidation (850 °C) and thermal stability (up to 1100 °C) [5]. An increase in the number of alloying elements, for example, by the combined addition of Al and Si to TiN, CrN and ZrN with the formation of multicomponent AlTiCrN, AlCrSiN, AlTiSiN, and ZrAlSiN, leads to a significant increase in thermal stability and mechanical characteristics compared to TiN, CrN, ZrN, TiAlN, and CrAlN [6–8]. In recent years, there has been a tendency to increase the number of constituent elements by more than 4 and the formation of nitrides of highly entropic alloys based on titanium nitride [9]. An important characteristic of such materials is lattice distortion [10], which manifests itself at the substructural level in an increase in microdeformation.

However, the highest properties were achieved when creating multilayer composites consisting of various nitride layers [11]. To increase the mechanical properties of TiN-based coatings, the addition of intermediate nanosized layers (the creation of multilayer nanocomposites) [12–14] with transition metal nitrides Cr, Zr, Mo, Nb showed high efficiency. To create such nanocomposite systems, the magnetron [15, 16] and vacuum-arc [17, 18] production methods are mainly used. The advantage of the vacuum-arc method is a high degree of plasma ionization [19], which allows one to obtain highly hard coatings with a thickness of more than 10 μm [20, 21].

Nanoscale multilayer coatings showed improved mechanical strength, hardness and wear resistance compared to single-layer coatings due to their structural state and a large number of interfaces between nanolayers.

It was found that the state of the interface between the layers and the thickness of the layers themselves can affect the microstructure and mechanical properties of

multilayer coatings. For example, blocking of dislocations by layer interfaces can lead to a significant increase in strength [22–24].

It was shown in [25] that for the AlTiCrN/TiSiN composite, the coherent growth of two types of materials, AlTiCrN and TiSiN, with different lattice constants, caused an alternating stress field, which improved the mechanical properties.

The aim of this work was to study the influence of the most effective technological parameters of the structural engineering of nanocomposites (displacement potential and layer thickness) on the structure, substructure, stress-strain state, and physicomechanical characteristics of (TiMo)N/(TiSi)N coatings.

SAMPLES AND RESEARCH METHODS

The coatings were deposited in the Bulat-6 vacuum-arc installation for 1.5 h at a working atmosphere pressure of $P_N = 4 \cdot 10^{-3}$ Torr. During the deposition process, a different negative bias potential (U_b) was supplied, which was -70, -110, and -200 V. The multilayer coatings were deposited from two sources of evaporation, one of which was TiSi (Si – 7 wt.%) the second is TiMo (Mo – 30 wt.%) in constant rotation mode (rotation speed 8 rpm) and in discrete mode (with a stop near each source from 10 to 160 s). Modes of obtaining coatings are given in Table 1, and the operation diagram of the installation during the deposition of (TiMo)N/(TiSi)N composites is shown in Fig. 1. The total thickness of the coatings was about 11 μm. The thickness of a single-layer coating of series 2 is about 9.3 μm, and that of series 4 is about 12 μm. With a total coating deposition time of about 90 min, this corresponds to a deposition rate of about 0.1 (TiSi)N and 0.13 μm/min (TiMo)N.

Table 1

Technological modes of deposition of coatings

Series No	Coating	P_N, Torr	U_b, V	Operating mode of the substrate holder
1	(TiSi)N	$4 \cdot 10^{-3}$	-70	mode constant rotation of the substrates
2			-200	
3	(TiMo)N		-70	
4			-200	
5	(TiSi)N/ (TiMo)N		-70	
6			-110	
7			-200	
8				10 s interval 530 layers
9				40 s interval 134 layers
10				80 s interval 68 layers
11				160 s interval 34 layers

The phase-structural state was investigated using X-ray diffractometry techniques. X-ray diffraction spectra were obtained on a DRON-4 setup in Cu-K_α radiation, using θ-2θ scanning in the range of angles 30...90º, with a scanning step of 0.1 deg and a holding time of 10 s. To monochromatize the detected radiation, we used a graphite monochromator installed in the secondary beam (in front of the detector) [26]. Complex profiles were divided into components using the "NewProfile" software package. To determine the phase composition of the coatings, we used the data of powder diffraction files (JCPDS) published by the International Center for Diffraction Data (ICDD) [27]. Substructural characteristics were determined by the approximation method [28].

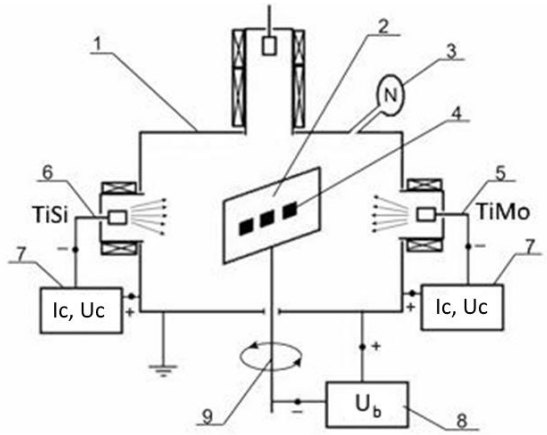

Fig. 1. The scheme of the installation during the deposition of (TiMo)N/(TiSi)N multilayer composites: 1 – vacuum chamber; 2 – metal screen; 3 – nitrogen leak; 4 – sprayed samples; 5 – TiMo evaporator; 6 – TiSi evaporator; 7 – arc sources; 8 is a source of supply of potential to the substrate; 9 – rotary mechanism

Surface morphology was studied using a Ziess AXIO Vert metallographic optical microscope A1.

Hardness was measured on a DM-8 microhardness tester (Affri, Italy) using a Vickers diamond pyramid as an indenter at a load of 50 g, exposure time 10 s. For each sample, 10 measurements were performed.

Revetest scratch tester (CSM Instruments) was used to determine the adhesion-cohesive strength, scratch resistance, and also to determine the fracture mechanism. Scratches were applied to the surface of the coatings under a continuously increasing load (from 0.9 to 190 N) at a loading speed of 15.76 N/min using a Rockwell C diamond spherical indenter with a radius of curvature of 200 μm. To obtain reliable results, three scratches 12 mm long were applied to the surface of each coated sample. At the same time, acoustic emission power, coefficient and friction force, indenter penetration depth, and normal load (FN) were simultaneously recorded.

RESULTS AND DISCUSSION

Figs. 2 and 3 show the surface morphology of single-layer (TiSi)N (see Fig. 2,a,b), (TiMo)N (see Fig. 2,c,d) coatings and multilayer composite (TiSi)N/(TiMo)N coatings.

From Figs. 2, 3 it is seen that with an increase in the bias potential, the number and size of the droplet phase decreases. Moreover, in a single-layer coating (TiSi)N, the amount of the drop phase is less than for (TiMo)N.

In (TiMo)N/(TiSi)N multilayer composites, the amount of the droplet phase decreases with increasing U_b.

As can be seen from the Cross-section of the images (Fig. 4), there are small inhomogeneities in the volume of (TiMo)N/(TiSi)N composites, however, the planarity of the layers is still quite good. The layers themselves have clearly defined boundaries, which indicates that even the supply of the highest U_b = -200 V does not lead to significant mixing of the layers.

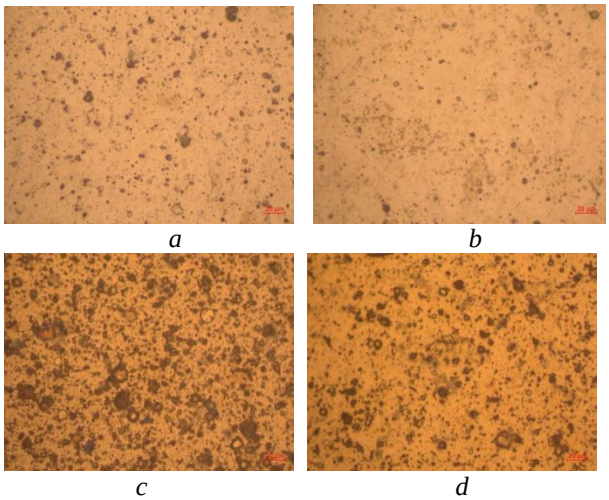

Fig. 2. Surface morphology of the single-layer (TiSi)N (a, b) and (TiMo)N (c, d): a, c – U_b = -70 V; b, d – U_b = -200 V

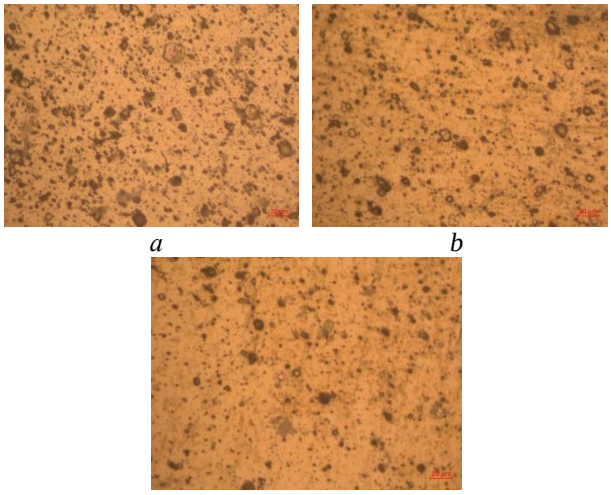

Fig. 3. Surface morphology of multilayer (TiSi)N/(TiMo)N coatings: a – U_b = -70 V; b – U_b = -110 V; c – U_b = -200 V

It can be seen that with a short deposition time of the layer with a large potential U_b = -200 V (series 7 and 8), the coating contains the smallest amount of Si. With an increase in the layer thickness of more than 80 nm (series 9–11), the Si content becomes about 1.7 at.%. Mo content in coatings varies. It should be noted that the content of elements in thick layers is close to that for small U_b (series 5).

The elemental composition was determined by X-ray fluorescence analysis [29]. The resulting data in at.% are shown in Table 2.

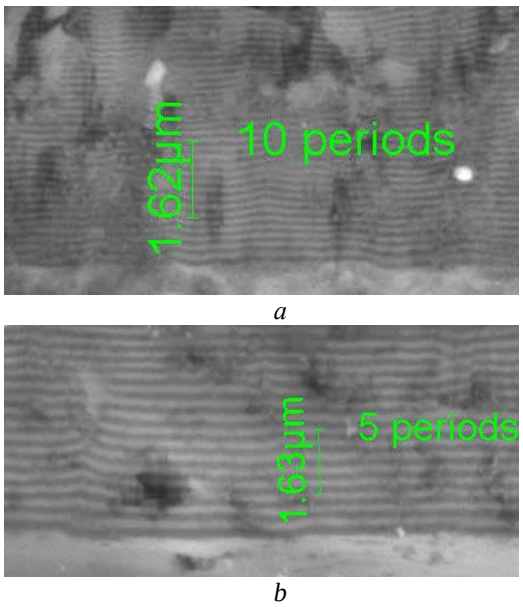

Fig. 4. "Cross-section" SEM images of coatings obtained at U_b = -200 V and a layer deposition time of 40 (a) and 80 s (b)

Table 2

The elemental composition of the studied coatings

Series No	Content, at.%		
	Ti	Mo	Si
1	97.106	–	2.894
2	97.827	–	2.173
3	86.391	13.609	–
4	87.446	12.554	–
5	94.133	4.124	1.743
6	94.345	4.219	1.436
7	95.259	3.862	0.879
8	93.924	5.627	0.449
9	91.130	7.075	1.795
10	93.295	4.946	1.759
11	93.046	5.365	1.589

To determine the phase-structural state in the work, the X-ray diffraction method was used.

Fig. 5 shows the X-ray diffraction spectra of single-layer coatings – (TiSi)N (see Fig. 5,a) and (TiMo)N (see Fig. 5,b), obtained at different negative bias potentials.

It can be seen from the X-ray diffraction spectra (see Fig. 5) that for (TiSi)N and (TiMo)N coatings, a single-phase state is formed based on TiN (JCPDS 38-1420) with an fcc crystal lattice (structural type B1 – NaCl). The supply of a large bias potential U_b = -200 V leads to a significant increase in the relative intensity of diffraction peaks from the {111} planes. This indicates an increase in the degree of perfection of the texture with the [111] axis perpendicular to the surface plane.

For (TiMo)N coatings, with an increase in U_b, a shift of diffraction peaks towards smaller angles is observed. Such a change is characteristic of the formation of compressive stresses in the coating [30]. Comparison of the spectra in Fig. 5, shows that, apparently, such stresses initiate heavy molybdenum atoms. This conclusion follows from the fact that for TiSiN (where the decisive influence is exerted by titanium atoms with the largest atomic mass), the displacement is much

smaller. The calculation of the lattice period from the position of the diffraction maxima (for the θ-2θ shooting scheme) led to the values: for TiMoN – 0.4309 nm (at U_b = -70 V) and 0.4325 nm (at U_b = -200 V); for TiSiN coatings, 0.4268 nm (at U_b = -70 V) and 0.4282 nm (at U_b = -200 V).

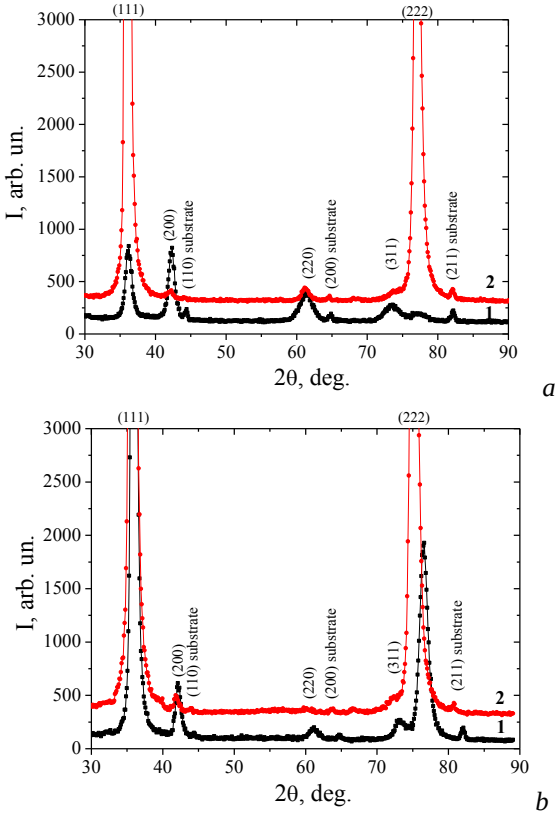

Fig. 5. XRD patterns of (TiSi)N (a) and (TiMo)N (b) coatings: 1 – U_b = -70 V; 2 – U_b = -200 V

To determine the stress – strain state in coatings with a strong texture, the method of crystalline groups was used [31, 32]. In the case of a texture with the [111] axis, the (333), (331), (420), and (511) planes were used as the base planes for studies. Filming was carried out at appropriate crystallographic angles. Typical "a-sin^{2}ψ" plots are shown in Fig. 6.

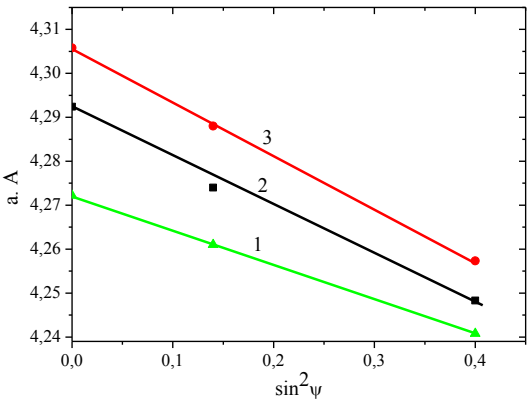

Fig. 6. "a-sin^{2}ψ" graphs of TiSiN coatings (1 – series 1); TiMoN (3 – series 2) and nanocomposite (TiSi)N/(TiMo)N (2 – series 7)

Fig. 6 shows that the lattice periods $a_\perp$ (sin^{2}ψ = 0) and a_{-40} (sin^{2}ψ ≈ 0.4) for (TiMo)N coatings are bigger than for (TiSi)N. In this case, the slope of the "*a*-sin^{2}ψ" plot for (TiSi)N is less than for (TiMo)N. The "*a*-sin^{2}ψ" plot for the (TiSi)N/(TiMo)N composite occupies an intermediate position (see Fig. 6, dependence 2).

The voltage graphs determined on the basis of the "*a*-sin^{2}ψ" data are compressive. Their value was -4.7 GPa for a single-layer coating (TiSi)N (series 2) and for a single-layer (TiMo)N coating -7.8 GPa (series 3) and -9.2 GPa (series 4). The lattice parameters are the smallest for (TiSi)N coating and the largest for (TiMo)N coating.

Figs. 7 and 8 show the sections of the diffraction spectra of (TiSi)N/(TiMo)N composite coatings obtained for different U_b (see Fig. 7) and layer thickness *h* (see Fig. 8).

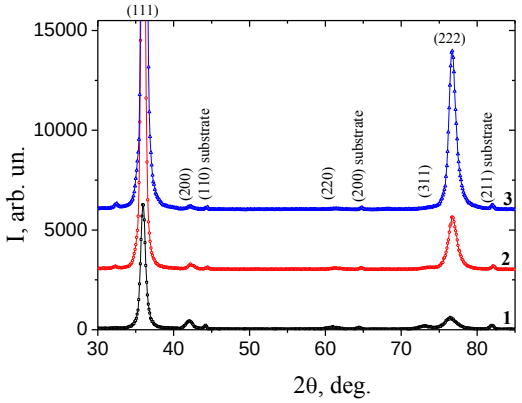

Fig. 7. XRD patterns of (TiSi)N/(TiMo)N coatings obtained at different bias potentials in the constant rotation mode: 1 – U_b = -70 V; 2 – U_b = -110 V; 3 – U_b = -200 V

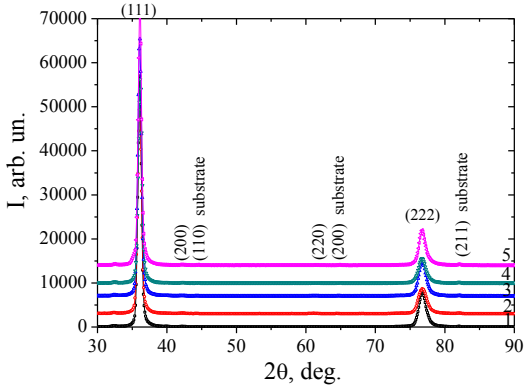

Fig. 8. XRD patterns of (TiSi)N/(TiMo)N coatings depending on the layer thickness (U_b = -200 V): 1 – h ≈ 350 nm; 2 – h ≈ 175 nm; 3 – h ≈ 80 nm; 4 – h ≈ 25 nm; 5 – h ≈ 11 nm

It is seen that multilayer coatings are characterized by the formation of the same type of crystal lattice (similar to the TiN phase, structural type B1-NaCl) as in single-layer coatings. In this case, up to the largest thickness *h* ≈ 350 nm (see Fig. 8, spectrum 1), in the multilayer composite (TiSi)N/(TiMo)N, there is no separation of peaks from (TiSi)N and (TiMo)N layers, which indicates the conservation quasi-epitaxial coupling at the boundary with the average lattice period [25, 33].

Fig. 9 shows graphs of the dependence of macrostresses on the bias potential and layer thickness.

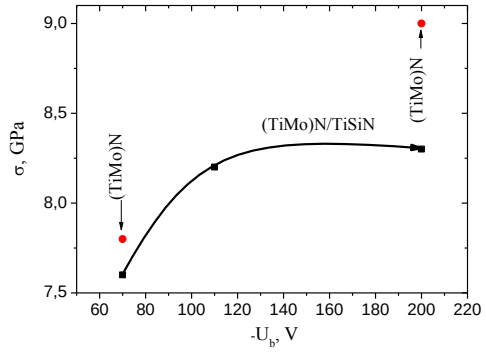

a

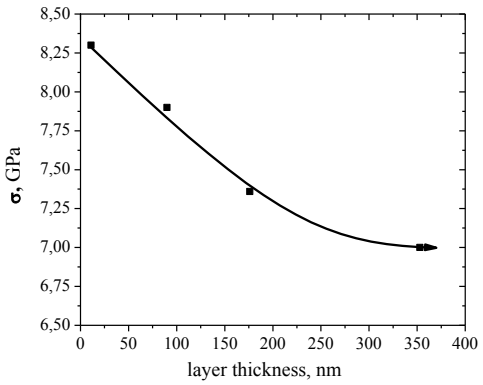

b

Fig. 9. Graphs of the dependences of macrostresses (σ) on the bias potential (a) and layer thickness – h (b) of multilayer coatings

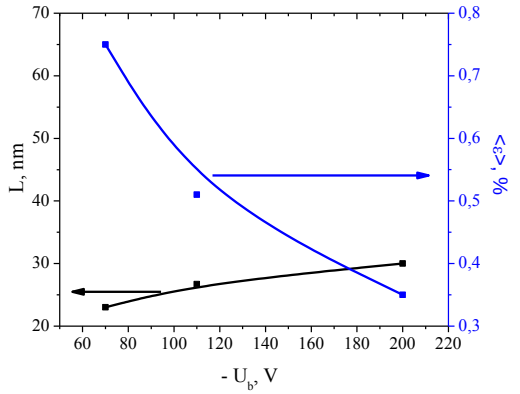

a

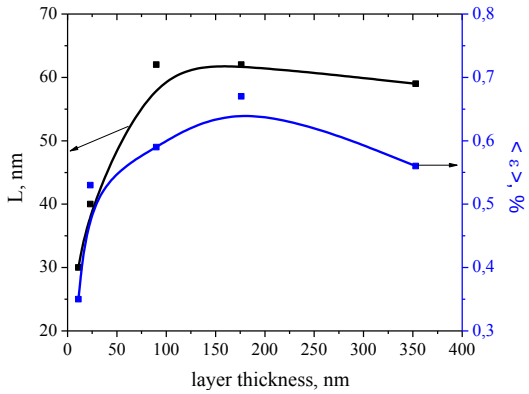

b

Fig. 10. Graphs of the dependences of the substructural characteristics of (TiSi)N/(TiMo)N coatings on the bias potential (a) and layer thickness – h (b)

It is seen that with an increase in U_b in the layers of the smallest thickness, the compressive stresses in the (TiSi)N/(TiMo)N composite increase. However, in absolute value, the stresses in the composite remain smaller compared to single-layer (TiMo)N coatings (see Fig. 9,a). With an increase in the thickness of the layer, the value of compression stresses decreases (see Fig. 9,b). With a maximum layer thickness of 350 nm, this decrease is about 20%.

Another important parameter in the analysis of diffraction spectra is the width of the diffraction lines. By changing the width of the diffraction lines, the substructural characteristics of the coating material were determined for different technological conditions for their preparation.

The calculation of the substructural characteristics (by the approximation method) showed that the crystallite size in a single-layer coating (TiSi)N is in the range 27...50 nm, with a microdeformation of ~ 0.44...1%, in a coating (TiMo)N – 42...63 nm, 0.43...0.63%, respectively. Substructural characteristics for multilayer coatings are shown in Fig. 10.

Fig. 10 shows that, with an increase in the bias potential, the crystallite size increases from 23 to 30 nm, which is explained by a slight heating of the surface. With an increase in the thickness of individual layers to 90 nm, an increase in crystallite size is observed. The crystallite size in the thinnest layers is 23...30 nm, which exceeds the layer thickness.

The reason for this may be the formation of a columnar microstructure [34] in epitaxially bound layers with an increased crystallite size in the direction of the texture axis [111].

To determine the mechanical properties of the coatings, microhardness was measured and scratch testing was carried out. The results of hardness measurements are shown in Fig. 11.

Single-layer coatings of (TiMo)N have a higher hardness in comparison with the (TiSi)N coating (see Fig. 11,a), which may be associated with a higher hardness of molybdenum.

In multilayer (TiSi)N/(TiMo)N coatings obtained in the continuous rotation mode (series 5–7), the hardness varies from 34.3 GPa (at U_b = -70 V) to 23 GPa (U_b = = -200 V with increasing bias potential). However, an increase in the layer thickness to 175 nm leads to an increase in hardness to 35 GPa. With a further increase in layer thickness, a decrease in hardness is observed.

Based on the data of microindentation, (TiSi)N/(TiMo)N coatings obtained at U_b = -70 V in continuous rotation mode, as well as at U_b = -200 V with a layer thickness of 80...175 nm, have the highest hardness. Fig. 12 shows wear paths for coatings having the highest hardness at critical loads L_{c1}...L_{c5}. So, the critical load corresponding to the cleavage of the coating or its plastic abrasion to the substrate (L_{c5}) corresponds to 135.72 N (U_b = -70 V, h = 11 nm), 166.09 N (U_b = -200 V, h = 80 nm), and 140.28 N (U_b = = -200 V, h = 175 nm).

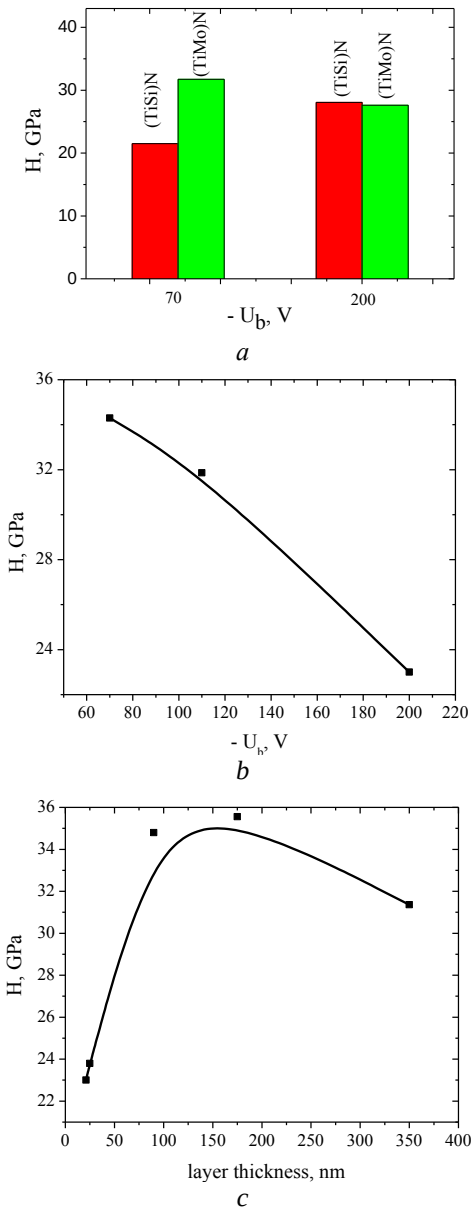

Fig. 11. Histogram of changes in hardness in single-layer (TiSi)N and (TiMo)N coatings (a) and the dependence of the hardness of multilayer (TiSi)N/(TiMo)N coatings on the bias potential in continuous rotation mode (b) and on the layer thickness at U_b = -200 V (c)

Characteristic of these coatings is the magnitude of compression macrostresses 7.3...7.7 GPa and microstrains 0.71...0.73%. Apparently, such a combination of the macrostressed state of the coating and the microdeformed state of crystallites allows one to achieve the highest strength characteristics in composite (TiSi)N/(TiMo)N multilayer coatings.

As can be seen from Fig. 12 plastic and uniform nature of wear allows to obtain high values of the parameters of cohesive fracture of the coating.

Thus, the coatings obtained at a layer thickness of 80 nm and U_b = -200 V have the highest hardness and strength; for this coating in Fig. 13 shows the results of sclerometry.

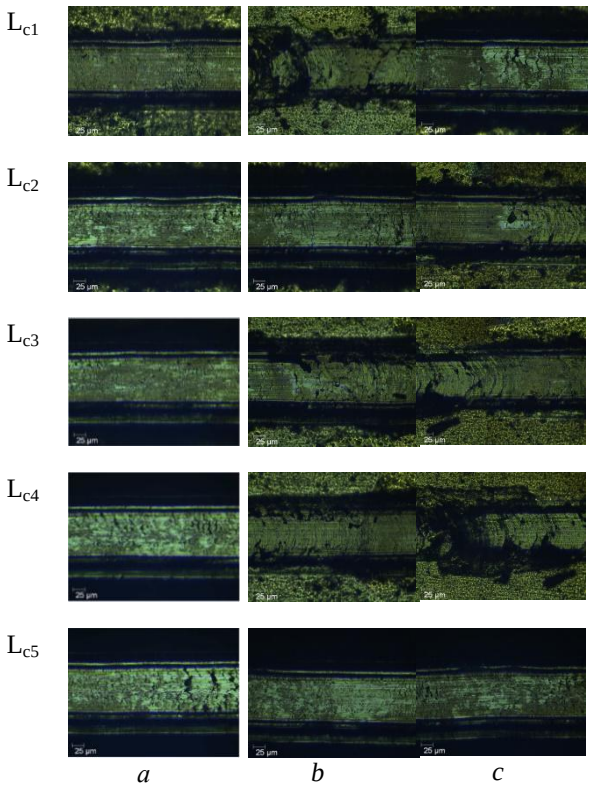

Fig. 12. Wear paths in the area of critical point loads (L_{c1}...L_{c5}): a – U_b = -70 V, h = 11 nm; b - U_b = -200 V, h = 90 nm; c – U_b = -200 V, h = 176 nm

As follows from the data in Fig. 13, a fairly uniform change in the main characteristics is observed with an increase in the load on the indenter. Wear of the coating occurs without the formation of avalanche chips, which confirms, in particular, the shape of the acoustic emission curve. The coefficient of friction as it deteriorates varies from 0.42 to 0.50.

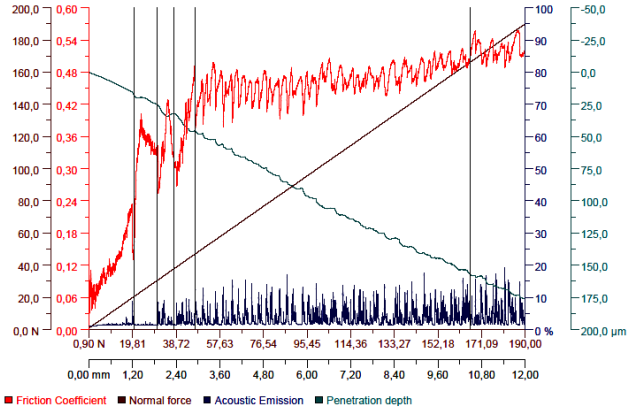

Fig. 13. Sclerometry results of (TiSi)N/(TiMo)N coatings obtained by U_b = -200 V, h = 80 nm

Thus, the (TiSi)N/(TiMo)N series of multilayer coatings obtained at U_b = -200 V and a layer thickness of 80 nm has the highest hardness of 34.8 GPa and adhesive strength of 166.09 N, which makes them promising for industrial applications as protective and functional elements of the surface of parts of engineering and power engineering equipment.

CONCLUSIONS

The research results showed that alloying titanium with molybdenum and silicon atoms and the formation of (TiMo)N and (TiSi)N layers on their basis leads to the formation of single-phase materials of the structural type B1-NaCl.

The hardness of such single-layer coatings does not exceed 30 GPa.

The creation of a multilayer composite (TiSi)N/(TiMo)N with a nanometer layer thickness can increase the hardness by more than 20% and at the same time achieve a high adhesive strength L_{c5} = 166.09 N.

From the perspective of structural engineering, the advantages of creating (TiSi)N/(TiMo)N multilayer composite include:

– of high structural macrostresses in the (TiMo)N component;

– a significant increase in hardness compared to the (TiSi)N component;

– the ability to vary widely the magnitude of microdeformation and crystallite size.

The features of the obtained composite (TiSi)N/(TiMo)N include the conservation of a single-phase state to relatively (about 350 nm) large layer thicknesses. This allows us to conclude that the presence of a mismatch of about 1% of the periods of (TiSi)N and (TiMo)N layers is not a critical value when creating a single-phase multilayer composite based on them.

Thus, the use of multielement (TiSi)N and (TiMo)N layers in a multilayer coating design allows one to achieve a high-strength state with high adhesive strength and good tribological characteristics.

The highest properties (hardness – 34.8 GPa and adhesive strength – 166.09 N) were achieved in coatings obtained at U_b = -200 V and a layer thickness of 80 nm, which are characterized by compression macrostresses of 7.85 GPa and microstrains – 0.75%.

REFERENCES

1. A. Venneman, H.-R. Stock, J. Kohlscheen, et al. Oxidation resistance of titanium–aluminium–silicon nitride coatings // *Surface and Coatings Technology*. 2003, v. 174, p. 408-415.

2. Y.-p. Feng, L. Zhang, R.-x. Ke, Q.-l. Wan, Z. Wang, Z.-h. Lu. Thermal stability and oxidation behavior of AlTiN, AlCrN and AlCrSiWN coatings // *International Journal of Refractory Metals and Hard Materials*. 2014, v. 43, p. 241-249.

3. V. Attari, A. Cruzado, R. Arroyave. Exploration of the microstructure space in TiAlZrN ultra-hard nanostructured coatings // *Acta Materialia*. 2019, v. 174, p. 459-476.

4. H. Söderberg, M. Odén, J.M. Molina-Aldareguia, L. Hultman. Epitaxial stabilization of cubic-SiN_x in TiN/SiN_x multilayers // *Appl. Phys. Lett*. 2005, v. 97, N11, p. 114327.

5. E.T. Norton Jr., C.C. Amato-Wierda. Kinetics and mechanism relevant to TiSiN chemical vapor deposition from TDMAT, silane and ammonia // *Surface and Coatings Technology*. 2001, v. 148(2-3), p. 251-255.

6. C. Tritremmel, R. Daniel, M. Lechthaler, P. Polcik, C. Mitterer. Influence of Al and Si content on structure and mechanical properties of arc evaporated Al–Cr–Si–N thin films // *Thin Solid Films*. 2013, v. 534, p. 403-409.

7. N. Ghafoor, I. Petrov, D.O. Klenov, B. Freitag, J. Jensen, J.E. Greene, L. Hultman, M. Odén. Self-organized anisotropic $(Zr_{1-x}Si_x)N_y$ nanocomposites grown by reactive sputter deposition // *Acta Materialia*. 2015, v. 82, p. 179-189.

8. J.P. Meng, L. Zhou. Enhanced thermal stability of ZrAlSiN cermet-based solar selective absorbing coatings via adding silicon element // *Materials Today Physics*. 2019, v. 9, p. 100131.

9. N.A. Azarenkov, O.V. Sobol, V.M. Beresnev, A.D. Pogrebnyak, D.A. Kolesnikov, P.V Turbin, I.N. Toryanik. Vacuum-plasma coatings based on the multielement nitrides // *Metallofizika i Noveishie Tekhnologii*. 2013, v. 35(8), p. 1061-1084 (in Russian).

10. P. Malinovskis, S. Fritze, L. Riekehr, L. von Fieandt, J. Cedervall, D. Rehnlund, L. Nyholm, E. Lewin, U. Jansson. Synthesis and characterization of multicomponent (CrNbTaTiW)C films for increased hardness and corrosion resistance // *Materials & Design*. 2018, v. 149, p. 51-62.

11. Q. Wan, B. Yang, H.D. Liu, J. Chen, J. Zhang. Microstructure and adhesion of MeN/TiSiN (Me = Ti, Cr, Zr, Mo, Nb_xAl_{1-x}) multilayered coatings deposited by cathodic arc ion plating // *Applied Surface Science*. 2019, v. 497, p. 143602.

12. O.V. Sobol′, A.A. Postelnyk, A.A. Meylekhov, A.A. Andreev, V.A. Stolbovoy, V.F. Gorban. Structural Engineering of the Multilayer Vacuum-Arc Nitride Coatings Based on Ti, Cr, Mo and Zr // *Journal of Nano- and Electronik Physics*. 2017, v. 9, issue 3, p. 03003-1–03003-6.

13. O.V. Sobol', A.A. Andreev, V.F. Gorban, A.A. Meylekhov, H.O. Postelnyk, V.A. Stolbovoy. Structural Engineering of the Vacuum Arc ZrN/CrN Multilayer Coatings // *Journal of Nano- and Electronic Physics*. 2016, v. 8(1), p. 01042.

14. O.V. Sobol', A.A. Meilekhov. Conditions of Attaining a Superhard State at a Critical Thickness of Nanolayers in Multiperiodic Vacuum-Arc Plasma Deposited Nitride Coatings // *Technical Physics Letters*. 2018, v. 44, p. 63-66.

15. Y.X. Ou, H.Q. Wang, B. Liao, M.K. Lei, X.P. Ouyang. Tribological behaviors in air and seawater of CrN/TiN superlattice coatings irradiated by high-intensity pulsed ion beam // *Ceramics International*. 2019, v. 45(18), p. 24405-24412.

16. B. Subramanian. Enhancement of biocompatibility of metal implants by nanoscale TiN/NbN multilayer coatings // *Journal of Nanoscience and Nanotechnology*. 2013, v. 13(7), p. 4565-4572.

17. V.N. Zhitomirsky. Structure and properties of cathodic vacuum arc deposited NbN and NbN-based multi-component and multi-layer coatings // *Surface and Coatings Technology*. 2007, v. 201(13), p. 6122-6130.

18. O.V. Sobol', A.A. Andreev, V.F. Gorban', V.A. Stolbovoy, A.A. Meylekhov, A.A. Postelnyk. Possibilities of structural engineering in multilayer

vacuum-arc ZrN/CrN coatings by varying the nanolayer thickness and application of a bias potential // *Technical Physics*. 2016, v. 61(7), p. 1060-1063.

19. I.I. Aksenov, A.A. Andreev, V.A. Belous, V.E. Strelnitskiy, V.M. Horoshih. *Vakuumnaya duga. Istochniki plazmyi, osazhdenie pokryitiy, poverhnostnoe modifitsirovanie.* K.: "Naukova dumka", 2012, 726 p. (in Russian).

20. O.V. Sobol', A.A. Andreev, V.F. Gorban. Structural engineering of vacuum-arc multiperiod coatings // *Metal Science and Heat Treatment*. 2016, v. 58(1), p. 40-42.

21. A.A. Andreev, O.V. Sobol', I.V. Serdyuk, N.V. Pinchuk, A.A. Metel, S.V. Fedorov, and N.Yu. Cherkasova. Regularities of the influence of the structural state of vacuum-arc-deposited TiN coatings on their resistance to abrasion // *Journal of Friction and Wear*. 2014, v. 35(6), p. 497-500.

22. S. Kowalski, M. Cygnar. The application of TiSiN/TiAlN coatings in the mitigation of fretting wear in push fit joints // *Wea*r. 2019, v. 426-427, p. 725-734.

23. Y.-Y. Chang, H. Chang, L.-J. Jhao, C.-C. Chuang. Tribological and mechanical properties of multilayered TiVN/TiSiN coatings synthesized by cathodic arc evaporation // *Surface and Coatings Technology*. 2018, v. 350, p. 1071-1079.

24. S.-M. Yang, Y.-Y. Chang, D.-Y. Lin, D.-Y. Wang, W. Wu. Mechanical and tribological properties of multilayered TiSiN/CrN coatings synthesized by a cathodic arc deposition process // *Surface and Coatings Technology*. 2018, v. 202, p. 2176-2181.

25. Y.-Y. Chang, Y.-J. Yang, S.-Y. Weng. Effect of interlayer design on the mechanical properties of AlTiCrN and multilayered AlTiCrN/TiSiN hard coatings // *Surface and Coatings Technology*. 2020, v. 389, p. 125637.

26. O.V. Sobol', O.A. Shovkoplyas. On advantages of X-ray schemes with orthogonal diffraction vectors for studying the structural state of ion-plasma coatings // *Technical Physics Lette*rs. 2013, v. 39 (6), p. 536-539.

27. http://www.icdd.com

28. I.C. Noyanand, J.B. Cohen. *Residual Stress Measurement by Diffraction and Interpretation*. Springer-Verlag, NewYork, 1987, 350 p.

29. I.F. Mikhailov, A.A. Baturin, A.I. Mikhailov, S.S. Borisova. Increasing the sensitivity of X-ray fluorescent scheme with secondary radiator using the initial spectrum filtration // *Functional Materials*. 2012, v. 19(1), p. 126-129.

30. O.V. Sobol'. Control of the structure and stress state of thin films and coatings in the process of their preparation by ion-plasma methods // *Physics of the Solid State*. 2011, v. 53(7), p. 1464-1473.

31. C. Genzel. X-Ray Stress Gradient Analysis in Thin Layers -Problems and Attempts at Their Solution // *Phys. Stat. Sol. (A).* 1997, v. 159, p. 283.

32. C. Genzel, W. Reinmers. A Study of X-ray Residual-Stress Gradient Analisys in Thin-Layers with Strong Filer Texture // *Phys. Stat. Solidi*: *A-Applied Research*. 1998, v. 166(2), p. 751-762.

33. O.V. Sobol', R.P. Mygushchenko, A.A. Postelnyk, E.V. Onoprienko, T.O. Syrenko, A.G. Men'shikov, A.V. Zvyagolskiy. Structural Engineering of the Growth of Crystallites with a Predominant Orientation in Bilayer Multi-Period Vacuum arc Nitride Coatings // *Journal of Nano- and Electronic Physics.* 2018, v. 10, N 3, p. 03009 (5 p.).

34. I.I. Aksenov, D.S. Aksenov, A.A. Andreev, V.A. Belous, O.V. Sobol. *Vakuumno-dugovyie pokryitiya. Tehnologiya, materialyi, struktura, svoystva*. Harkov: NNTs HFTI, 2015, 379 s. (in Russian).

Article received 02.03.2020

ВЛИЯНИЕ ВЕЛИЧИНЫ ПОТЕНЦИАЛА СМЕЩЕНИЯ И ТОЛЩИНЫ СЛОЕВ НА СТРУКТУРУ, СУБСТРУКТУРУ, НАПРЯЖЕННО-ДЕФОРМИРОВАННОЕ СОСТОЯНИЕ И МЕХАНИЧЕСКИЕ ХАРАКТЕРИСТИКИ ВАКУУМНО-ДУГОВЫХ МНОГОСЛОЙНЫХ (TiMo)N/(TiSi)N-ПОКРЫТИЙ

О.В. Соболь, А.А. Постельник, А.А. Мейлехов, В.В. Субботина, В.А. Столбовой, А.В. Доломанов, Д.А. Колесников, М.Г. Ковалева, Ю.В. Сухорукова

Для создания многослойного композита использованы слои на основе нитрида титана, легированного молибденом и кремнием. При этом несоответствие периодов решеток (TiMo)N- и (TiSi)N-слоев составило около 1%. Установлено, что в многослойном композите (TiMo)N/(TiSi)N такое несоответствие периодов в составляющих слоях не изменяет однофазного состояния композита даже при относительно больших толщинах слоев (около 350 нм). Создание (TiMo)N/(TiSi)N-композита с нанометровой толщиной слоев позволяет уменьшать величину макронапряжений (большая величина которых свойственна однослойным (TiMo)N-покрытиям) и в широком интервале значений изменять субструктурные характеристики. Установлено, что использование многоэлементных (TiMo)N- и (TiSi)N-слоев при многослойном дизайне покрытий позволяет достичь высокотвердого состояния с высокой адгезионной прочностью и хорошими трибологическими характеристиками. Наиболее высокие свойства (твердость – 34,8 ГПа и адгезионная прочность – 166,09 Н) были достигнуты в покрытиях, полученных при U_b = -200 В и толщине слоя 80 нм, для которых характерна величина макронапряжений сжатия 7,85 ГПа и микродеформации – 0.75%.

ВПЛИВ ВЕЛИЧИНИ ПОТЕНЦІАЛУ ЗСУВУ І ТОВЩИНИ ШАРІВ НА СТРУКТУРУ, СУБСТРУКТУРУ, НАПРУЖЕНО-ДЕФОРМОВАНИЙ СТАН І МЕХАНІЧНІ ХАРАКТЕРИСТИКИ ВАКУУМНО-ДУГОВИХ БАГАТОШАРОВИХ (TiMo)N/(TiSi)N-ПОКРИТТІВ

О.В. Соболь, Г.О. Постельник, А.О. Мейлехов, В.В. Субботіна, В.О. Столбовий, А.В. Доломанов, Д.О. Колесніков, М.Г. Ковальова, Ю.В. Сухорукова

Для створення багатошарового композиту використані шари на основі нітриду титану, легованого молібденом і кремнієм. При цьому невідповідність періодів решіток (TiMo)N- і (TiSi)N-шарів становила близько 1%. Встановлено, що в багатошаровому композиті (TiMo)N/(TiSi)N така невідповідність періодів у складових шарах не змінює однофазного стану композиту навіть при відносно великих товщинах шарів (близько 350 нм). Створення (TiMo)N/(TiSi)N-композиту з нанометровою товщиною шарів дозволяє зменшити величину макронапружень (більша величина яких властива одношаровим (TiMo)N-покриттям) і в широкому інтервалі значень змінювати субструктурні характеристики. Встановлено, що використання багатоелементних (TiMo)N- і (TiSi)N-шарів при багатошаровому дизайні покриттів дозволяє досягти високотвердого стану з високою адгезійною міцністю і гарними трибологічними характеристиками. Найбільш високі властивості (твердість – 34,8 ГПа і адгезійна міцність – 166,09 Н) були досягнуті в покриттях, отриманих при U_b = -200 В і товщині шару 80 нм, для яких характерна величина макронапружень стиску 7,85 ГПа і мікродеформації – 0,75%.